11

Welding of Thin Light Alloys Sheets by CO_2 Laser Beam: Magnesium Alloys

Afia Kouadri-David
PSM Team, European University of Brittany, France, INSA of Rennes, LGCGM France

1. Introduction

Laser welding is an important joining technique for magnesium alloys with their increasing applications in aerospace, aircraft, automotive, electronics and other industries. In this document the research and progress in laser welding of magnesium alloys are critically reviewed from different perspectives. Some important laser processing parameters and their effects on weld quality are discussed. The microstructure, metallurgical defects and mechanical properties encountered in laser welding of magnesium alloys, such as porosity, grains size, crystallographic texture and loss of alloying elements are described. Mechanical properties of welds such as hardness, residual stresses and other important structural properties are discussed. The aim of the chapter is to review the recent progress in laser welding of magnesium alloys and to provide a basis for follow-on research.

2. General principle of laser beam welding

Laser Beam Welding (LBW) consists in the laser beam focalisation on the workpiece surface. The high power density then created, induces metal ionisation and then plasma is formed. The vaporisation of the surface progressively forms a depression in the workpiece and then a keyhole, which allows the laser energy in-depth absorption. The melted metal will progressively fill the keyhole during the laser displacement, to form the weld. The two laser sources available are CO_2 and Nd: YAG. Laser CO_2 consists in a mixture of CO_2, N_2 and noble gases. The nitrogen discharges in CO_2 molecules activate the laser emission. The Nd: YAG (neodymium-doped yttrium aluminium garnet) consists in Nd^{3+} ions inserted in YAG crystal, the excitation is supplied by laser diodes. Nd: YAG laser light (λ = 1.06 µm) has a much higher absorption degree than CO_2 laser light (λ=10.6 µm). Both CO_2 and Nd:YAG lasers operate in the infrared region of the electromagnetic radiation spectrum, invisible to the human eye. The Nd:YAG provides its primary light output in the near-infrared, at a wavelength of 1.06 microns. This wavelength is absorbed quite well by conductive materials, with a typical reflectance of about 20 to 30 percent for most metals. The near-infrared radiation permits the use of standard optics to achieve focused spot sizes as small as .001" in diameter. On the other hand, the far infrared (10.6 micron) output wavelength of the CO_2 laser has an initial reflectance of about 80 percent to 90 percent for most metals and requires special optics to focus the beam to a minimum spot size of .003" to .004" diam. However, whereas Nd:YAG lasers might produce power outputs up to 500 watts, CO_2

systems can easily supply 10,000 watts and greater. The two laser processes are differentiated by the fabrication and the shape of the beam. It is generally accepted that the heat input parameter, defined as the ratio of beam power to beam travel speed, is well suited for describing LBW process. However, our results and those of the literature show that this parameter was not convenient, and that, the effect of the laser power and the welding speed parameters have to be differentiated, in particular for the light alloys such as magnesium or aluminium alloys. As a result of these broad differences, the two laser types are usually employed for different applications. The powerful CO_2 lasers overcome the high reflectance by keyholing, wherein the absorption approaches blackbody. The reflectivity of the metal is only important until the keyhole weld begins. Once the material's surface at the point of focus approaches its melting point, the reflectivity drops within microseconds.

3. Optimisation and influence of CO_2 laser beam parameters on thin sheets

The present investigation is concerned with laser power, welding speed, defocusing distance and type of shielding gas and their effects on the fusion zone shape and final solidification structure of magnesium alloys.

3.1 Laser power, P (kW)

The laser power is a critical parameter to obtain a full penetration depth and to control the weld bead profile. High power density at the workpiece is crucial to achieve keyhole welding and to control the formation of welds. Studies realized in this domain showed this effect of laser power on the penetration depth and weld width. The increasing beam power led to deeper and wider beads. Figure 1 shows the effect of laser power on the penetration depth (Fig. 1A) and weld width (Fig. 1B) for WE43 alloy welded at a speed of 33 mm/s and a focused diameter of 0.25mm (Dharhi et al., 2001a, 2001b as cited in Cao et al., 2006).

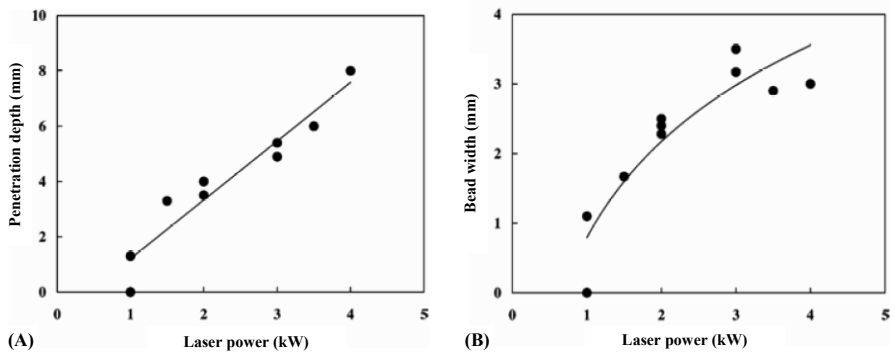

Fig. 1. Influence of laser power on the penetration depth (A) and on the weld width (B) for WE43 alloy (Dharhi et al., 2001a, 2001b)

The penetration depth and weld width increased with increasing laser power due to higher power density. Our experiences showed too the same evolution: the weld width becomes larger with increasing laser power. For example the threshold power to achieve full penetration is 2,5 kW (i.e. a power density of 2 MW/cm^2) for 3 mm AZ91 plates welded at a speed of 4 m/min and a focused diameter of 0.25 mm.

Then, when laser power was too low, lack of penetration was observed whereas high laser power produced laser cutting. These observations are consistent with the LBW literature. From macrostructure point of view, many authors observed the same evolutions where at low beam powers, some chevronlike pattern which is also called "ripples" (Marya et al., 2001). The mechanism of ripples formation is related to the effects of surface tension on the weld pool during solidification (D'Annessa, 1970 as cited in Cao et al., 2006). They also observed that the thickness in the weld area was slightly higher, a phenomenon which is called "crowning" or "humping". High beam powers led to deep and wide beads, and reduce both ripples and crowning (Marya et al., 2001). However, others authors showed at high beam powers, spatters and the evaporative losses would be produced. Authors (Weisheit et al., 1997) investigated the laser parameters for several magnesium alloys. They reported that for thin AZ31 plates (1, 8 mm), a 1.5 kW beam power was sufficient for achieving full penetration. In our experiences, for achieving full penetration, 3 mm AZ91 plates welds were produced at 4 kW (Kouadri & Barrallier, 2006).

3.2 LBW welding speed, V (mm/min)

The penetration depth and weld width both increase linearly with decreasing welding speed and decrease with increasing welding speed. The obtained results in the literature and reported on the figure 2A and 2B confirm the effects of welding speed on penetration depth and weld width at different levels of power for CO_2 lasers: The penetration depth and weld width both decrease linearly with increasing welding speed.

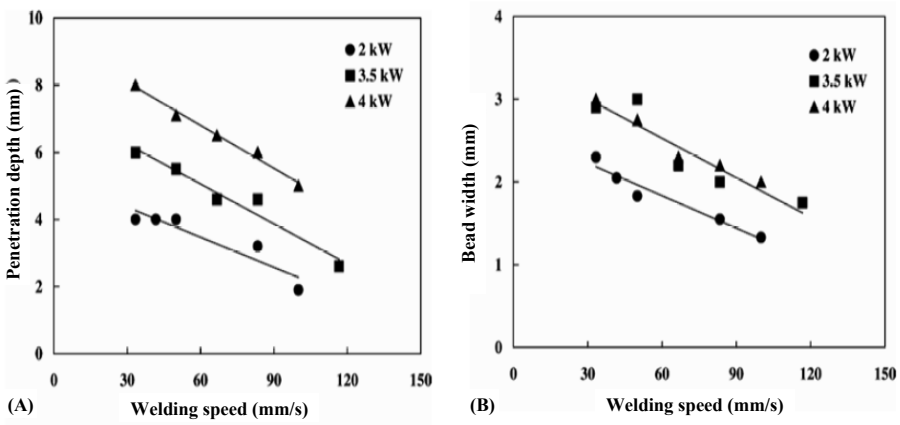

Fig. 2. Influence of welding speed on the penetration depth (A) and on the weld width (B) for WE43 magnesium alloy (Dharhi et al., 2001a, 2001b)

Moreover, it was reported that the speed lead too either to improve or to decrease the weld quality, in particular by the formation of the defects such as cracking or the pores formation.

Indeed, at low speeds, the interaction time between molten metal and surrounding air is large enough to allow pores to nucleate in large quantity, grow and escape from the molten pool as a result of buoyancy and convection flow. Moreover, when the welding speed is too slow, the bead produced by the superfluous heat exchange will extend to the side, and the

heat influenced area will become too heat and extended, the seam metallographic structure crystal becomes thick, sometimes the cracking will appear, which will seriously influence the welding quality. When the welding speed achieves the lower limitation, the superfluous power absorption also will induce local evaporation loss and hollows. Moreover, using lower welding speeds induced no real change in the penetration depth but wider the weld width and especially the heat affected zone (HAZ) (Marya & Edwards, 2000).

From pores formation point of view, at high speeds, the pores do not have enough time to nucleate. The influence of the welding speed on pore formation was studied (Marya & Edwards, 2001). They found that the pore fraction goes to a maximum with increasing welding speed. The obtained results showed that using higher welding speeds reduced ripples but greatly increased crowning phenomena (Marya & Edwards, 2001), and the fusion zone appeared to be far more brittle (Watkins, 2003 as cited in Cao et al., 2006). Moreover, they showed a dependency between crowning and pores content, so that crowning is actually a relevant parameter to assess the weld quality. When welding speed was too high, lack of penetration was observed, whereas low welding speed produced laser cutting. This one is explained by the fact the power density increases with decreasing welding speed (Dharhi et al., 2000 as cited in Cao et al., 2006).

However these observations must be readjusted because the results depend on the nature of used magnesium alloys. Indeed, though similar welding parameters are used, various magnesium alloys exhibit different welding performance due to their different metallurgical and thermophysical properties. For example, die cast AZ91D has a lower thermal conductivity of 51 W/m K as compared with 139 W/m K for wrought AZ21A alloy. Thus, for similar welding parameters, the AZ91D alloy has a higher weld depth and weld volume compared with AZ21A alloy. It was also reported that greater penetration depth could be reached in AM50 alloy compared with AZ91 alloy welded under similar conditions using a 6kW CO_2 laser (Marya & Edwards, 2001). These observations explain why it is needed to systematically investigate the laser-welding characteristics of different magnesium alloys because of the difference in their thermal properties. In the same way, it is needed to take account of the geometry and thickness of the plates for readjusting the speed of welding. Many authors reported that a welding speed of 2.5-3 m/min was suitable for thin plates, when using 1.5 kW laser beam. Therefore, welding speed above 3 m/min should be achievable during CO_2 laser welding of 2 mm thick plates (Weisheit et al., 1997).

3.3 LBW density (W/cm^2)

It's the one more important parameter: the power density is one of most pivotal parameters in laser weld. When the laser power density is lower than 10^6 W/cm^2, the laser weld belongs to category of heat exchange weld. When the laser power density achieves only 10^6 W/cm^2, the deep penetration weld can be formed and "keyhole effects" appears.

The "keyhole effects" is closely correlative to the laser power density which is more low, the "keyhole effects" is more unstable even can not be formed, and the melting pool is also small. The melting depth of laser weld is directly correlative to the laser output power density and which is the function of incidence beam power and beam diameter. Therefore, to enhance the power density, we can enhance laser power or decrease the laser speed. A good balance had to be found to avoid laser cutting when the power density was too high

and lack of penetration when the power density was too low. Concerning LBW, increasing the laser power (P) and decreasing the welding speed (V) result in an increase of the power density. This tendency is consistent with all the previous studies on laser welding.

3.4 Beam diameter

This is also a very important technical parameter, because in a certain output power, it will decide the density of beam power which is the key factor for laser weld. But for the laser beam with high power, it is difficult to measure, what is produced by the nature of the beam diameter. For laser weld, the condition of high effective deep penetration weld is that the power density on the laser focus must exceed 10^6 W/cm^2. We can adopt two methods to enhance the power density, one is to enhance the laser power, and the other one is to reduce the diameter of the beam. The power density has linear relation with the laser power, and has inverse-square ratio relation with beam diameter, so the effect of reducing beam diameter is better. In ours experiments, to realize full deep penetration weld of 2mm thick plates, we choose beam diameter of 1 mm with 4 kW CO_2 at 3 m/min.

3.5 LBW focal distance, f (mm)

For the sake of simplicity, the focal distance is defined as the distance between the focal point and the top surface of the sample. The position of focal points has an important influence on welding process and quality. The focal plane should be set where the maximum penetration depths or best process tolerances are produced. The laser welding usually needs some focus distance, because too high power density of the beam center at the laser focus is easy to vaporize and become bores. When the focus distance reduces to a certain value, the melting depth will suddenly change, which will establish necessary conditions for producing penetration pores. These most results in this domain showed that the focus distance influences not only the laser beam on the weld piece surface, but also the incidence direction of beam, so it has important influences to the melting depth and seam shape.

In our experiences, the most acceptable weld profile was obtained at defocusing distance of – 0.2 mm for 3 mm thickness where weld bead depth / width ratio is maximum and fusion zone size is minimum. In order to obtain the optimum value, complete penetration butt welds were made using previously obtained optimum laser power (4 kW) and optimum welding speed (3 m/min) (Kouadri & Barrallier, 2006). Sound welds were achieved with a focal point on the surface, which is consistent with what we found for thin plates. The weld width increases with moving the focal point away from the surface (i.e. increasing focal distance) which was also observed by other authors. These results indicated that the most effective range of defocusing distance to get maximum penetration with acceptable weld profile lies between zero and – 1 mm.

However, this distance has to be adjusted to obtain the best quality of welding. For example, the optimum defocusing distance to attain acceptable weld profile for 5 mm thickness was 0.4 mm under the surface of the workpiece (Cao et al., 2006). These results were consistent with the literature study (Dharhi et al., 2000, 2001, 2002 as cited in Cao et al., 2006). They studied 1–5kW CO_2 laser welding of 2mm AZ91 and 4mm WE43-T6 alloys. Their results showed that an adequate weld could be obtained for a focal position on or 1mm under the

surface of the workpiece. Focal position on the workpiece surface had the smallest weld width while the weld width became larger when the focal position deviated above or below the surface.

Then, the optimal focal point position to weld thin plates lies on the top surface of the workpiece. Indeed, Weisheit et al., (1997, 1998) investigated 2.5kW CO_2 laser welding of some magnesium alloys. For thin plates (2.5 and 3 mm), the best welds according to penetration depth, aspect ratio and sag were achieved when the focal point was adjusted on the surface of workpiece, whereas for thick plates (5 and 8 mm) a position of 2mm below the surface of workpiece proved to be the best. Thus, the focal position should be moved deeper into the material for thicker work pieces and the following used process. Lehner et al., 1999 further researched the tolerance of focal position. For 3mm AZ91 and AM50 die castings welded using a 3 kW Nd:YAG laser, the best focal position is approximately 0.8mm below the workpiece surface, with a tolerance of ±0.5 mm. For 5mm material, the focal position has to shift to about 1.2±0.2mm below the surface.

3.6 LBW shielding gas flow, V (l/min)

Shielding gas selection produces a best weld quality. With the welding laser, the welding gas is flushed onto the workpiece through a nozzle system in order to protect molten and heated metal from the atmosphere. Gases have different chemical reactions and physical properties, which affect their suitability as assist gases for different welding tasks. At least three important points must be considered: tendency to form plasma, influence on mechanical properties and shielding effect.

Three main types of shielding gases are used: helium, argon and nitrogen. Helium is a gas characterized by minimum molecular weight, maximum thermal conductivity, and maximum ionization energy, thereby making it the most suitable gas for suppressing plasma formation. Argon, on the other hand, becomes ionized relatively easily and is therefore more prone to forming excessive amounts of plasma, in particular at CO_2 laser power over 3 kW. Carbon dioxide and nitrogen, on the other hand, are reactive gases, which may react with the weld metal to form oxides, carbides, or nitrides and get trapped in pores. This can result in welds with deficient mechanical properties. As a result, pure carbon dioxide or nitrogen are unsuitable as welding gases in certain applications in particular for the aluminium or magnesium alloys due to the oxidation.

To reduce the plasma effect, in these cases, it is advantageous to use inert gases such as helium or argon as welding gases, because there is no reaction on the weld metal and do not affect weld metallurgy. Indeed, in general, when the laser beam interacts with the workpiece, a hole is drilled through the thickness of the material. This hole or cavity is filled with plasma and surrounded by molten metal, thus, the high energy density of the focused beam could be lost easily. Weisheit et al., 1997 investigated the effectiveness of these three shielding gases and reported that a helium gas flow was the best choice. This plasma effect was reduced as a result of the higher ionization potential of helium, and then the weld profile was improved.

These welding gases have other functions, too. It protects the focusing optics against fumes and spatters and, in the case of CO_2 lasers, also controls plasma cloud formation. Leong et al., 1998 when welding 1.8 mm thick AZ31B-H4 used helium top shielding gas to protect

from oxidation, combined with helium back shielding and nitrogen shielding to protect the optics. Wang et al., 2006 studied the influence of gas flow rate on weld width and reported that increasing gas flow up to 20 l/min is needed to affect the susceptibility to oxidation.

As magnesium is highly susceptible to oxidation, a protective atmosphere is required during welding. Surface cracking leading to laser welding was observed without gas protection. This is due to the oxide formation during welding in the magnesium alloys. To increase the magnesium alloy weldability, argon or helium are the most common choices. Argon is heavier than air so it provides a better shield than helium, but it ionizes easily and has much lower thermal conductivity than helium. This causes a problem with high power CO_2 welding: The metal vapour emerging from the keyhole is partially ionized, with charged atoms and free electrons. The free electrons absorb some of the laser light, reducing the power available for welding. As the vapor absorbs energy, it heats up, increasing the number of free elections and further increasing absorption. Helium shield gas is more effective than argon in suppressing this effect because it cools the vapor plume and does not contribute many electrons itself. This welding gas often plays an active role in the welding process, such as increasing the welding speed and improving the mechanical properties of the joint. Weisheit et al., 1997 investigated the effectiveness of these three shielding gases and confirmed that a helium gas flow was the best choice.

In addition, often to increase the weld quality, helium/argon mixtures combining the benefits of both gases, i.e. the higher density of argon and the higher ionization potential of helium, may be used to obtain better protection of the weld zone in CO_2 laser welding. Hiraga et al., 2001 studied 1.7 mm thick AZ31B-H24 butt joints and get some improvements using argon back shielding in addition to the helium centre shielding. With these two gases, weld profile is remarkably improved where fusion zone interfaces are almost parallel to each other. The melting depth increases with the increase of gas flux, but too much gas flux will induce the surface hollow even penetration of the melting pool. Indeed, higher porosity content was observed for He gas flow higher than 50 l/min. Using Ar back shielding gas allowed us to produce sound welds at lower welding speed, reducing sag of the weld pool. Our study led to the same conclusions and sound welds were produced (Kouadri & Barrallier, 2006). Then, the optimum shielding system consists in a top helium flow superior to 20 l/min and Ar back shielding. By adding single-sided access, laser welding is even more strategically advantageous.

4. Application of laser beam CO_2 on thin sheets of magnesium alloy

The presented material is a cast magnesium alloy (AZ91D) welded by laser CO_2 processing. The alloy used for the study of the laser welding is a ternary magnesium - aluminium - zinc of designation AZ91, according to standard ASTM. Laser welding of magnesium alloys appears to be a challenge itself. Indeed, the ability to produce laser welds depends on the properties of the material to be welded. Then, magnesium being characterised by quite unfavourable properties (i.e. low absorptivity of laser beams, strong tendency to oxidize, high thermal conductivity, high coefficient of thermal expansion, low melting temperature, wide solidification temperature range, high solidification shrinkage, a tendency to form low melting-point constituents, low viscosity, low surface tensions, high solubility for hydrogen in the liquid state), processing is expected to be an issue.

The used magnesium alloy in this study were obtained by high pressure die casting under neutral gas and did not undergo heat treatment to match the conditions generally encountered in automobile applications. The provided plates were sheared to recover 3-mm-thick samples. Their edges were machined by milling. The plates were welded together side by side using a laser beam CO_2, which penetrated through the thickness of the plates. The welding was performed using a 4000 W CO_2 laser in an inert helium atmosphere. The speed of welding was optimised in the range of 1.0 – 4.25 m/min and the power in the range of 1 – 4 kW.

The objective of this part is to show the evolutions of the metallurgical and mechanical properties generated by the laser CO_2 in thin AZ91 magnesium alloy sheets. The presented results were obtained with optimized parameters of CO_2 laser beam welding. This part shows the microstructure modifications (characterization of the grain size, chemical properties and the crystallographic texture) occurring during laser welding in every zone of the welded sheet. From mechanical properties point of view, we present the evolution of the hardness and the residual stresses. These one have been performed by taking into account the crystallographic texture. The strain measurements and the characterization of the crystallographic texture have been performed using X-ray diffraction techniques. The set of results demonstrated that laser welding induces the presence of several distinct zones which have distinct microstructural and mechanical properties.

4.1 Study of metallurgical properties

4.1.1 Macrostructure analysis

From macrostructure point of view, a narrow weld joint is an important characteristic of high power density welding. The 4 kW CO_2 laser welding in an inert helium atmosphere (2 bars) with a speed of welding of 2 m/min of 3mm AZ91D plates showed that the fusion zones have widths of approximately 0.8 1.6 mm (Kouadri & Barrallier, 2006). The region with a width of about 200 – 500 μm between the base metal (BM) and the fusion zone (FZ) can be recognized as the heat affected zone (HAZ). However, the width of the HAZ is defined according to the variations of laser beam parameters. For example, in the literature, the 6 kW CO_2 laser welding with a speed of welding of 3.5 m/min of wrought AZ31B alloy indicated that the width of the HAZ was 50–60 μm, but can be doubled at substantially slower speeds (Leong et al., 1998; Sanders et al., 1999). These results showed that the width of the HAZ is tightly connected to laser process parameters.

4.1.2 Microstructure analysis

From microstructure point of view, the microstructure of the laser welds is characteristic of a high-speed process in which heat is rapidly extracted from the molten fusion zone by surrounding base material. In our study, the mean grain sizes of the base metal (BM) range from 50 to 200 μm (figure 3a).

The BM is heterogeneous and characterised by a mixture of a large primary α-Mg phase and of a (α-Mg + β-$Mg_{17}Al_{12}$) eutectic phases. This later constituent is a so-called abnormal eutectic (Kouadri & Barrallier, 2006, 2011; Dubé et al., 2001; Luo, 1996) because of its lamellar shape. The base metal exhibits small precipitates dispersed in the matrix but mainly located at the grain boundaries. These precipitates are β-$Mg_{17}Al_{12}$ and to a lesser degree

Al_8Mn_3. The typical overall microstructure of the HAZ is shown in figure 3b. The microstructure of HAZ has coarse grain polygonal Mg as the base metal. Nevertheless, eutectic grains disappeared whereas a continuous β-$Al_{12}Mg_{17}$ phase was created at grain boundary. At the fusion boundary, where a relatively large thermal gradient and small growth rate are established, the microstructure is predominantly cellular (Marya & Edwards, 2000). Grains usually grow epitaxially from the Fusion Zone (FZ) –Heat Affected Zone (HAZ) interface.

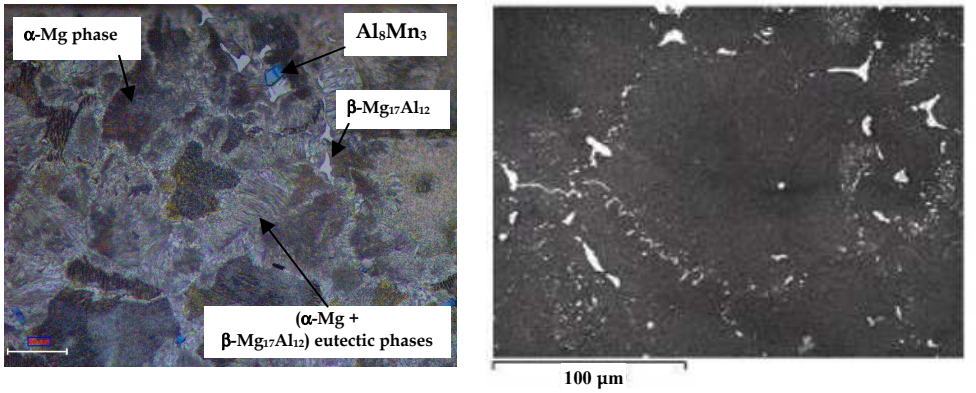

Fig. 3. a) Microstructure of the base metal, solid solution α-Mg and (α-Mg + β-$Mg_{17}Al_{12}$) eutectic phase and precipitates (OM), b) Microstructure of the Heat Affected Zone (HAZ) by SEM (Kouadri & Barrallier, 2006, 2011)

In the fusion zone (FZ), the microstructure is very different from the base metal (Figure 4a, 4b).

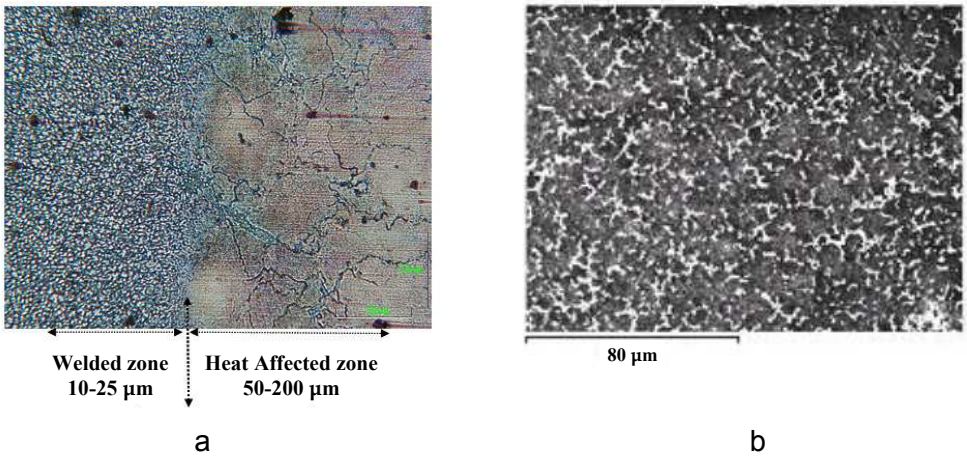

Fig. 4. a) Microstructure in the welding zone and in the heat affected zone by (OM), b) Microstructure of the fusion zone (SEM) (Kouadri & Barrallier, 2006, 2011)

The α-Mg microstructure is much finer ranging between 10µm and 25µm. There is β-$Mg_{17}Al_{12}$ precipitates too, clearly present and located in grain boundaries. So, the microstructure appears to be more homogenous at scale lengths of a few micrometers. This fine equiaxed grains in the fusion zones formed by cellular growth were also observed by the others authors (Cao et al., 2006) in Zr-containing ZE41A alloy. Weisheit et al., 1997, 1998 have also observed a cellular morphology in all joints except for the WE54 alloy which showed a more globular grain shape. It was further observed the equiaxed morphology in AM60B alloy occurring at low welding speeds. At higher welding speeds, however, the morphology changes from equiaxed to dendritic forms (Pastor et al., 2000). In the same way, our observations showed that the rapid cooling experienced during laser welding leads to a significant grain refinement with cellular growth in the fusion zone. In brief, the laser welding leads to a grain refinement some is the initial structure (Haferkamp et al., 1996, 1998). Only the grain morphology changes following the used laser parameters. Indeed, it was reported that the original microstructure has little influence on the fusion zone structure though magnesium alloys can be welded in different conditions (Weisheit et al., 1998).

4.1.3 Distribution of grain size and volumetric fractions of phases by image analysis

An example of the statistical distribution of the different grain sizes obtained by grain count is presented on the figure 5a.

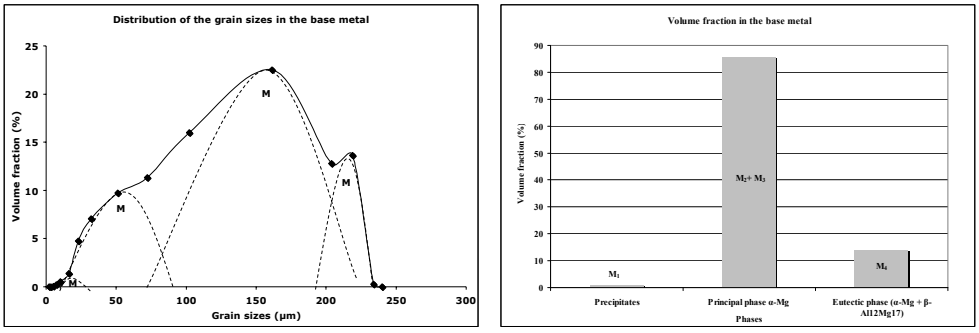

Fig. 5. (a) Statistical distribution of the grain sizes of AZ91 alloys in the base metal. (b) Volume fraction of the α-Mg grains, of the eutectic (α-Mg grains β-$Mg_{17}Al_{12}$) phase and of the precipitates in the base metal (Kouadri & Barrallier, 2011).

This distribution shows the presence of four modes; M_1, M_2, M_3 and M_4: The precipitates (M_1), whose main mode is about 10 µm and the principal α-Mg (M_2 + M_3) phase, whose main modes are 50 and 160 µm. Finally the principal mode of the eutectic phase (α-Mg + β-$Al_{12}Mg_{17}$) is about 220µm. The volumetric fractions calculation (figure 5b) demonstrates that the volumetric fraction of the base metal for the principal α-Mg phase is estimated at 85.4%, that of the eutectic phases at 13.8% and those of the precipitates at 0.8%. These results are in line with those in the literature and the diagram of the alloy phase AZ91 (StJohn et al., 2003). The large reduction of grains in the fusion zone is confirmed by statistical distribution of the grains (Figure 6a) where the principal mode is 16µm. The volumetric fraction of the principal phase represented by modes 2 and 3 constitutes 96% of the matrix (Figure 6b). The eutectic phase has almost disappeared in the welded zone.

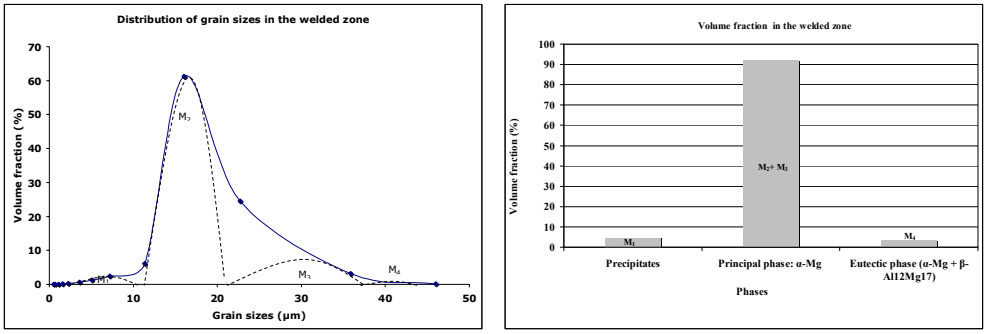

Fig. 6. a) Statistical distribution of the grain sizes of AZ91 alloys in welded zone, b) Volume fraction of the α-Mg grains and of the β-$Mg_{17}Al_{12}$ precipitates in the welded zone (Kouadri & Barrallier, 2010).

4.1.4 Chemical analysis

Generally, the laser welding leads to the redistribution of chemical composition or evaporative losses in the fusion zone. In the case of magnesium alloys, the temperatures reached within keyholes are far greater than the boiling temperatures of magnesium, aluminium or zinc (Liu et al., 2000). Thus, during welding, the preferential evaporative losses consist primarily of zinc and magnesium and then aluminum. This evaporation causes a variation of chemical composition in the fusion zone, especially at high laser power density which leads to a new chemical redistribution.

In our studies, the welding of AZ91 D plates, the chemical composition (% weight.) of each individual phase in the different phases was studied using EDS analysis. The base metal constitutes a reference state for the comparison with the welded area. In the table 1 energy dispersive spectroscopy (EDS) analysis indicated that the α-Mg grain contains up to 8.1 and 1.15 wt. % of Al and Zn, respectively. The α-phase contains ≈ 32 wt. % Al (Kouadri & Barrallier, 2006). All these results were in complete agreement with the literature on AZ91 alloy microstructure, which has been widely studied.

Chemical Composition (weight %)		Al	Mg	Zn	Mn	Fe	Si
Base metal	Matrix α, $(\alpha+\beta)$	8,1	90,6	1,15	0,15	-	-
	Precipitates β	32,5	67,5	-	-	-	-
	Precipitates Al_8Mn_3	32,8	14,5	-	52,7	-	-

Table 1. Chemical composition of AZ91 alloy in base metal, BM, (EDS analysis) (Kouadri & Barrallier, 2006).

The tables 2 and 3 show the evolution of the chemical composition in the HAZ and in the welded zone.

In the HAZ, higher Al and Zn concentrations in the α-phase were measured as compared to the base metal and to the welded zone (Kouadri & Barrallier, 2006). So, this confirms that β-$Mg_{17}Al_{12}$ and Al_8Mn_3 precipitates were diluted in a matrix made of over-saturated α-phase.

In the welded zone, the chemical composition of phases was much the same as in base metal (Kouadri & Barrallier, 2006) except in a thin superficial layer close to the surface. The Al-content in the β-phase decreases from 30 % (weight) in the BM down to 17% (weight) in the fusion zone. Likewise, we could see a strong decrease of the Al-content in every crystalline phase. We did'nt observe evaporative losses due to a good optimisation of the laser parameters. Indeed, it is known that higher energy densities lead to greater evaporative losses, increased spatter, and uneven weld beads. Thus, minimizing the irradiance incident upon the workpiece would reduce the loss of high vapor pressure elements. For example, larger reductions of both Mg and Zn were also reported at slower travel speeds (Leong et al., 1998; Sanders et al., 1999). We can conclude in the case of the magnesium alloys that there aren't evaporative losses of Mg and Zn if the laser parameters are optimized. There is only a chemical redistribution of the overall Al quantity for example in our case, due to the solidification conditions (Kouadri & Barrallier, 2006, 2011; Dubé et al., 2001; Luo, 1996). This redistribution should then be carefully controlled and optimized by manipulation of welding parameters.

Chemical Composition (weight %)		Al	Mg	Zn	Mn	Fe	Si
HAZ	Matrix α	8,51	90,31	1,15	0,04		-
	Precipitates β	26,83	69,63	3,50	0,04		-

Table 2. Chemical composition of AZ91 alloy in the HAZ, (EDS analysis) (Kouadri & Barrallier, 2006).

Chemical Composition (weight %)		Al	Mg	Zn	Mn	Fe	Si
welded zone	Matrix α	8,3	90,3	1,1	0,2	-	0,1
	Precipitates β	29,9	69,1	-	-	-	-

Table 3. Chemical composition of AZ91 alloy in welded metal, (EDS analysis) (Kouadri & Barrallier, 2006).

4.1.5 Texture characterisation

In general, texture develops in a metal as a result of processes such as crystallisation, plastic deformation…. The practical importance of preferred crystallographic orientation results from the dependence of many mechanical and physical properties on crystal direction. Thus, a textured material will have, in general, anisotropic values for a number of parameters including the yield strength, Young's modulus and Poisson's ratio. In order to understand how preferred crystallographic orientations might occur in laser welding, it is necessary to consider the formation and structure of the fusion zone in detail.

Initially, in our study, the base metal is characterized by a random orientation. Likewise, there is no more texture in the HAZ with 90% of the grains being randomly oriented. This is consistent with Coelho et al., 2008, study. In the fusion zone, the microstructure consists of fine and randomly oriented equiaxed dendrites nucleated. The texture analysis showed clearly that there is no texture. Indeed, ODF calculation indicates that more than 99% of the grains are randomly oriented (Kouadri & Barrallier, 2006, 2011).

However, close to the surface, the AZ91 alloy exhibits two preferential orientations concerning 77% of the grains (Figure 7a).

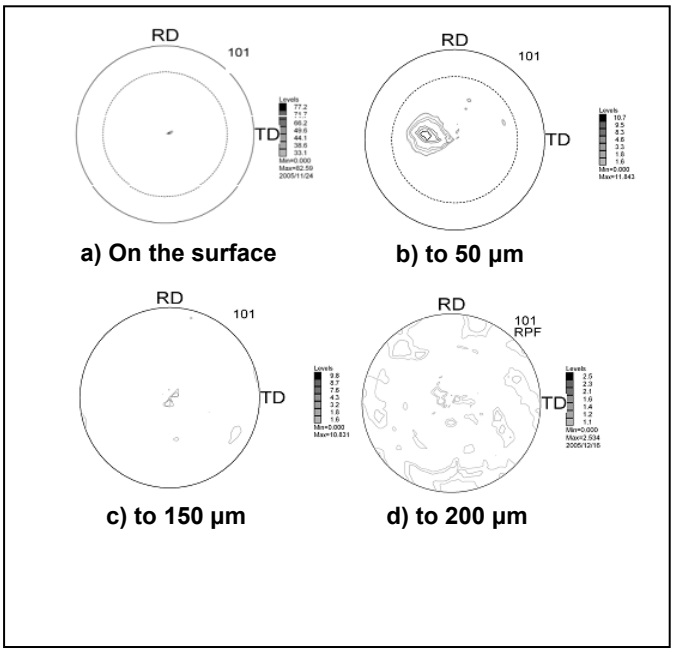

Fig. 7. Evolution of the crystallographic texture (pole figure 101) from the surface to a depth of 200 µm: a) Texture to the surface, b) Texture to 50 µm, c) Texture to 150 µm, d) Texture to 200 µm (Kouadri & Barrallier, 2006, 2011).

The $\{10\bar{1}1\}$ pole figure showed that a large fraction of grains are oriented with pyramidal $\{10\bar{1}1\}$ planes parallel to the surface of the sheet. The intensity of the center of this pole figure is a tenfold improvement in intensity compared with other peaks. A close look at the position reveals that the normal axis is tilted at an angle of ± 4° from the normal sheet direction to the transverse direction and around the welding direction. The ODF calculation allows us to say that 71% of the grains have an orientation $\{10\bar{1}1\}\langle\bar{3}4\bar{1}3\rangle$ corresponding to the 3 Euler angles (φ_1 = 65,6°, ϕ = 60,8°, φ_2 = 54,4°). Likewise, the $\{10\bar{1}0\}$ pole figure shows the presence of a smaller proportion of grains with $\{10\bar{1}0\}$ planes parallel to the surface. Such grains show two other poles $P_i^{\{10\bar{1}0\}}$ and $P_j^{\{10\bar{1}0\}}$, on both sides of the centre, due to the multiplicity of the hexagonal symmetry, which is equal to three. These poles are tilted at 60° around the centre. The ODF calculation allows us to say that 6% about of the grains have an orientation $\{10\bar{1}0\}\langle0\bar{3}34\rangle$ corresponding to the 3 Euler angles (φ_1 = 65°, ϕ = 90°, φ_2 = 60°). The most likely explanation for the variation of texture between the surface and the depth of the fusion zone is that the differences of the thermophysical and thermomechanical properties of the investigated location affect the process of solidification and plastic deformation, leading to different final out-comes. In our study, the nature of this texture has been explained by the thermodynamic conditions of minimisation of surface energies

(Kalinyuk et al., 2003; Matysina, 1999) which results in the presence of columnar grain growth at the surface of the welded zone (Kurtz et al., 2001). Between the surface and the 200 µm depth (Figure 7b, 7c, 7d) the texture decreases to disappear completely from 200 µm. This change underlines the presence of a transition from columnar growth to equiaxial grain growth. These results showed that the laser welding led to a complex microstructure and induced high temperature and deformation gradients which may cause changes in crystalline orientations. The study of the texture evolution is then required to understand the anisotropic characteristic of the welds and its influence on mechanical properties. Compared with the literature, little study takes into account the texture due to laser welding. So our results showed that the laser welding can form a crystallographic texture and that it is necessary to study it thoroughly to apprehend the mechanical properties as well as possible.

4.2 Experimental results of the mechanical properties

4.2.1 Hardness characterization

From laser parameters point of view, hardness in the fusion zone was found to increase almost linearly with welding speed because higher welding speeds lead to a more significant refinement of the microstructure and more alloying elements into the matrix, even though hard intermetallics are reduced and more finely distributed at high cooling rates. The average hardness of CO_2 laser welded joints decreases with slower welding speeds. Indeed, at low welding speeds the weld structure and hardness were nearly the same or sometimes lower as those in the base die-cast material. The decrease in the hardness of the HAZ was due to grain growth. However, these results depend too on the laser power and the nature of used alloy. In the literature, it was also reported that there was a gradual decrease in hardness of 6 kW CO_2 laser welded joints from the BM to the HAZ to the FZ of AZ31BH24 alloy, with a minimum value in the FZ (Leong et al., 1998; Sanders et al., 1999). Dhahri et al., 2001 investigated WE43-T6 alloy using 5 kW CO_2 laser. The hardness at the top and bottom of the welds was similar but the hardness in the middle of the bead was lower. In our studies, the 4 kW CO_2 laser welding of die cast AZ91D alloy showed that there is an increase in hardness of the fusion zone but little variation in hardness occurs in the HAZ according to the localization of the measurements. Figure 8 shows an example of the hardness results, measured close to the surface on both sides of the linear weld in a profile including the base metal passing through the heat affected zone and the welded zone. The same measurement has been realized along the same profile and at a depth around 200 µm.

Close to the surface, the hardness varies from around 90 HV in the base metal and around 95 HV in the heat affected zone to 110 HV in the welded zone. The hardness in the HAZ is higher than in the BM, even though the size of the grains is identical. This augmentation of microhardness has in part been explained by the contribution of added elements and particularly the increase in the level of aluminium in this zone (10%). Other studies have also demonstrated the presence of precipitates which are formed in this zone considered to be a zone of diffusion which contributes towards augmenting the hardness (Shaw et al., 1997). In the fusion zone, compared to the base metal, the increase in hardness was probably

due to its finer microstructure and higher volume fraction of intermetallics such as $Mg_{17}Al_{12}$ (Watkins, 2003).

Of the same form, through the thickness at a depth around 200 µm, the results show a different evolution than the surface concerning the BM and the HAZ, the hardness is lower. In the depth, the evolution of the microhardness shows no statistical variation of the microhardness between the base metal, the heat affected zone and the welded zone contrary to the surface. We can see that the hardness between the base metal, the heat affected zone and the core of the welded zone at a depth around 200 µm stays stable with a value of about 85 HV. Though significant grain coarsening occurred in the HAZ of AZ91 alloy, the hardness in the HAZ was still almost the same as that in base metal. These results join those of literature. Weisheit et al., 1997, studied 2.5kW CO_2 laser welding of cast magnesium alloys such as AZ91 AM60, ZC63, ZE41, QE22 and WE54 and wrought alloys (AZ31, AZ61, ZW3 and ZC71). For as-cast alloys, there is an increase in hardness of the FZ but little variation in hardness occurs in the HAZ. These observations demonstrate that laser welding induces particular profiles in the zones studied. These differences in hardness distribution over laser weld joints indicate the inhomogeneity of the joints following used parameters. Hardness is influenced by the laser welding parameters but too the initial chemical composition and also depends on the manufacturing process of the magnesium alloy. The choice of the laser process CO_2 or Nd:YAG influences too the hardness. This last point has been demonstrated by Hiraga et al., 2001, studied 2 kW CO_2 and Nd:YAG laser welding of wrought AZ31B-H24 butt joints of 1.7mm thickness. Their results showed that the Nd:YAG laser welded fusion zone is slightly harder than the FZ produced by CO2 laser.

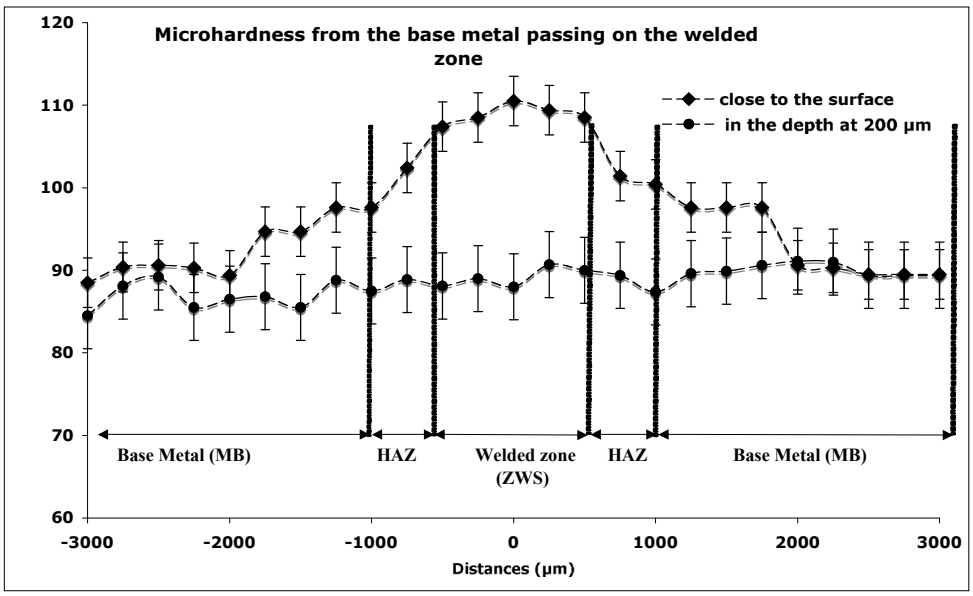

Fig. 8. Hardness from the base metal passing on the heat affected zone and the welded zone close to the surface and in the thickness at a depth about 200 µm (Kouadri & Barrallier, 2011).

4.2.2 Residual stresses results

The origin of residual stresses and their evolution within a welded joint is difficult to evaluate because they are the result of a number of competing mechanisms: shrinkage changes in phase and microstructure (Dai & Shaw, 2003). In our case, the magnesium alloy does not undergo a phase transformation, as is the case for aluminium alloys. Numerous studies have shown that when this is the case residual stresses are primarily a consequence of an inhibited shrinkage in the weld line and of the modified microstructure which is linked to strong temperature gradients, and to their distribution within the material (Wagner, 1999; Cho et al., 2003; Mao et al., 2006).

4.2.2.1 Distribution of the residual stresses at the surface of the assembled sheets

The measurements were undertaken in the welded zone, perpendicular to the weld line towards the base metal. Figure 9 shows an example of the obtained results.

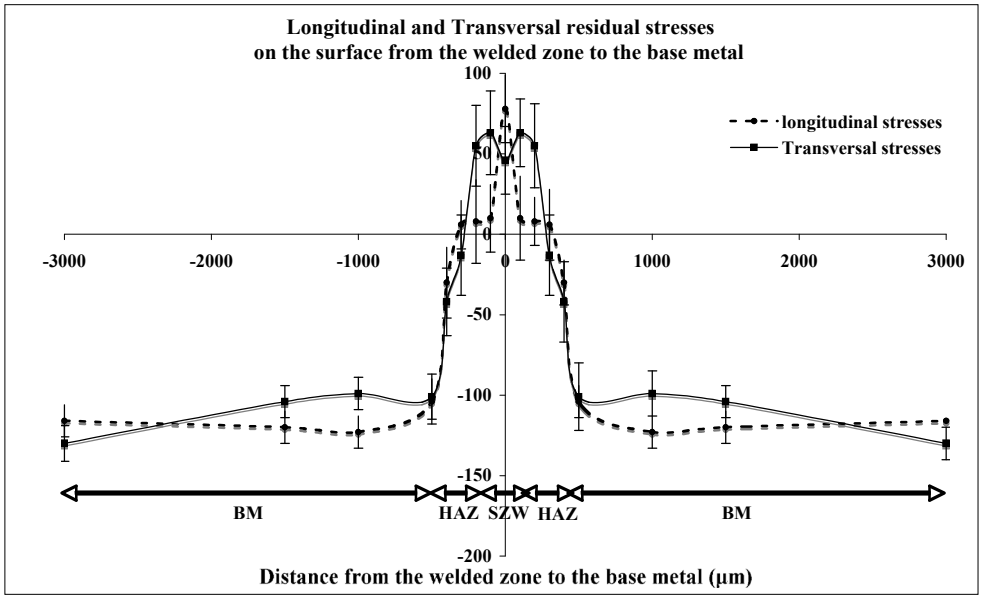

Fig. 9. Longitudinal and transverse residual stresses close to the surface from the base metal until the welded zone (Kouadri & Barrallier, 2011)

At the surface, the results demonstrated that the base metal presents a state of compression, whereas the weld line is submitted to residual traction stresses. This state of compression has been attributed to the nature of the cooling, linked to the moulding process. With laser welding, cooling occurs by the diffusion of heat through the outer surfaces of the plates which are in contact with the mould walls. Furthermore the machining by milling of the surface of the base metal before welding accentuates the state of compression and explains the raised values (- 120 MPa) observed at the surface of the base metal. However, in the weld line the heat is evacuated by the plates and not the free surfaces. This leads to traction

stresses. This evolution is in line with mechanical equilibrium. The welded zone exhibits residual traction stresses which are counter balanced by compression stresses in the base metal (Pryds & Huang, 2000).

Furthermore, study of the state of surface stresses demonstrates some anisotropy: the residual stresses are not equibiaxial. We observe that the longitudinal component decreases from the center of the weld zone towards the base metal, whereas the transverse component remains high before a sudden reduction. These changes occur in the thermally affected zone, and are associated with numerous factors and by many authors with a zone of relaxation. The evolution of the longitudinal stress can be connected with the heat flow resulting from the mobile heat source that follows the welding direction. We can see two explanations of these evolutions. On the one hand, the effect of temperature and cooling speed gradients arise from the anisotropic heat flow (Teng et al., 2002), on the other, the anisotropy can be the result of a shrinking structure. The negligible thermal dilation of both plates prevents the free shrinkage of the weld line along the direction of the weld line. The same applies to the transverse component. The restricted shrinkage in the transverse plane arises from the clamping of the plates during welding. Even if the influence of the clamping is hard to evaluate experimentally, digital studies have shown that the field of residual stresses is strongly influenced by the geometry of the assembly (Jensen et al., 2002; Dai & Shaw, 2003).

4.2.2.2 Distribution of the residual stresses though the thickness of the welded zone

The profiles of the average stresses through the thickness are plotted in the figure 10 for the longitudinal and transversal residual stresses.

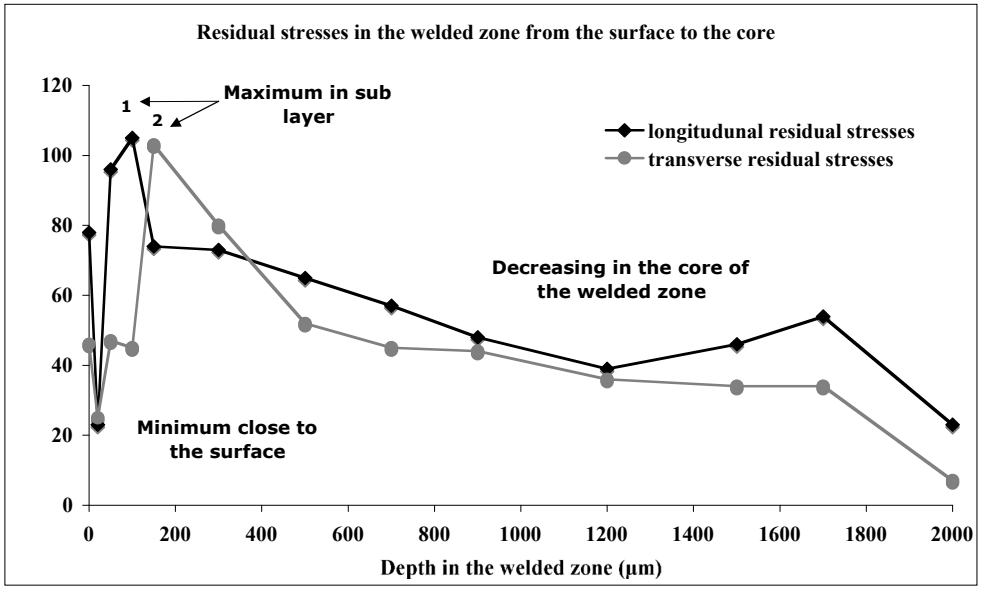

Fig. 10. Longitudinal and transverse residual stresses from the welded zone close to the surface to the core of the welded zone (Kouadri & Barrallier, 2011)

The study through the thickness of the welded zone shows that in general the profiles of the stresses reproduce the asymmetry of the welding process. Their behaviour in tension and their variation have in part been explained by the influence of the thermal cycle on the origin of residual stresses and their evolution within the material. The residual stresses on the face exposed to the laser beam are elevated (up to 80 MPa) whereas the opposite face creates stresses of only 23 and 7 MPa respectively for the longitudinal and transverse stresses. This effect can also be explained by the fact that using inert gas ensures very rapid cooling of the superior face whereas the inferior face cools more slowly (Dong et al., 2004).

Finally we have noticed that over the first 200 micrometers the residual stresses present a particular evolution. The intensity of the stresses is not maximum at the surface of the welded zone (78 and 45 MPa respectively for the longitudinal and transverse constraints) as expected, but at a depth of 200µm the stress is 100 MPa. The presence of this maximum stress demonstrates that there is a stress gradient between the textured layer and the heart of the isotropic welded zone. This specific evolution has partly been explained by the plastic deformation of the superficial layer. By presenting a strong texture and an important loss of aluminum, the superficial layer is more sensitive to plastic deformation in the plane compared to the heart of the weld line which is isotropic (Hsiao et al., 2000). These results can be compared to a thin coat deposit because these thin coatings are textured and the maximum stresses are found at the interface (Pina et al., 1997; Cevat Sarioglu 2006).

In our study there is a transition zone with a continual evolution in properties, in particular an evolution of the texture between the outer surface and the depth at about 200 µm. It appears that the development of this texture affects the distribution of stresses with a relaxation of the stresses at the surface and a maximum in the under layer. We explain these modifications by the fact that the level of plastic flow, related to local stresses, is dependent on grain orientation (Su et al., 2002; Agnew & Duygulu, 2005; Wu et al., 2007).

In conclusion, these results showed that the laser welding processes influence the residual stress distribution. Whereas compressive stresses are obtained in the base metal, tensile stresses are obtained in the LBWelds due to thermal gradients and high residual stresses are observed in the LBW fusion zone. These results showed too that it is important to take into account the crystallographic texture to evaluate the residual stresses.

5. Conclusions

The influence of various welding parameters during continuous wave CO_2 laser beam welding of thin plates of magnesium alloys was investigated in this chapter. It is known that the weldability of such materials is usually not excellent and lasers can be utilized to achieve good quality welds. The obtained results and the realized synthesis from the literature showed that the CO_2 laser welding possesses comprehensive performances such as good technology and the technology of laser welding magnesium alloys plates is well appropriated. The keyhole welding mode is likely to be encountered in the laser welding of thin sheet magnesium. The results of a detailed investigation showed the influence of different parameters of the laser which have to be tightly combined to obtain a weld quality.

However, during laser welding of magnesium alloys, therefore, some processing problems and weld defects can be encountered such as an unstable weld pool, substantial spatter a strong tendency to drop-through for large weld pools (Leong et al., 1998; Haferkamp et al., 1998; Sanders et al., 1999), sag of the weld pool (especially for thick workpiece), undercut (Dubé et al., 2001), porous oxide inclusions, loss of alloying elements (Leong et al., 1998; Sanders et al., 1999), excessive pore formation (particularly for die castings) (Pastor et al., 2000; Zhao & DebRoy, 2001) and solidification cracking (Marya & Edwards, 2000). These defects are generally decreased by a good optimization of the laser parameters. In view of the results achieved in this study, the use of high-power intensity focused CO_2 laser beam with optimized parameters and careful material preparation prior to welding can produce welds with high quality for the most magnesium alloys, in particular for AZ91D of our study (Kouadri & Barrallier, 2006, 2010). Welding speed of 2 m/min and laser power of 4kW let to a full penetration of 3mm thickness welded joint. Optimum weld profile was obtained when focal point was placed on the top surface. In comparison with the literature, all the investigated magnesium alloys showed tendencies for porosity and solidification cracking particularly, at high welding speed (≥4m/min). Porosity was prevented by accurate cleaning of the base metal before welding and optimizing the flow rate of argon shielding gas. In order to maintain the mechanical properties when welding magnesium alloys, the heat input and time of exposure to very high temperatures must be minimized. For LBW, the laser power (P) and weld speed (V) directly influence the heat input. This relationship is often used to determine the heat input.

Beyond of the optimization of laser parameters, it is believed that the efficiency of CO_2 laser beam welding of magnesium alloys could be improved by cleaning the workpiece surface prior to welding. This is due to increasing surface roughness that means decreasing surface reflectivity and enhancing the laser energy coupling during welding. Recent efforts on $C0_2$ laser beam welding have resolved several of the initial problems associated with the welding of magnesium alloys. Consistent and repeatable welds can now be obtained without resorting to meticulous edge preparation. Moreover, elimination or reduction of the plasma is recommended for optimal welding of magnesium. This effect of plasma formation which affects the weld quality and the optics during welding has been clarified: trouble-free operation of the optics has been achieved with the use of inert gas shielding such as helium.

However, several results showed that the weldability of thin magnesium plates was significantly better with the Nd:YAG laser. These observations were attributed to the higher absorption of the Nd:YAG beam, which in turn reduced the threshold irradiance required for welding and produced a more stable weldpool. Indeed, an advantage of Nd:YAG laser processing is its shorter wavelength; consequently, because of the dependency of the material's emissivity on the wavelength, energy is absorbed by the material more readily than for the CO_2 laser and a lower energy can be used for welding, allowing greater control of the heat input. This is particularly useful when working with thin materials. Recently, tremendous efforts have been made to clarify the fundamental laser weldability of different types of magnesium alloys using both Nd:YAG and CO_2 lasers. It is pointed out that improvements in the laser weldability of a range of magnesium alloys are possible by increasing the power density of the focused spot, and this can be achieved through higher average powers, improved beam focusing system, and decreasing beam reflectivity on

workpiece surface. In conclusion, the weldability problems of magnesium alloys are much more easily overcome when using Nd:YAG than CO_2 laser. However, our studies showed that CO_2 laser is more appropriate to weld cast magnesium alloy than wrought magnesium alloy.

From technology point of view, in comparison with the traditional welding method such as arc welding processes, the laser welding has high efficiency, small welding distortion, low labor costs and convenient construction, is easy to realize automatization, and can be the effective measure to enhance the weld quality. Laser welding processes offer great benefit over other welding processes, e.g., arc welding, resistance welding, etc., since less heat is coupled into the workpiece. The low-heat input will tend to keep a very narrow HAZ then, retaining some to the strength of the material. The benefits of low-heat input and extremely rapid cooling rate, all of which help to minimize the metallurgical problems in the fusion zone. For example, high cooling rate will tend to slow down the development of blisters because of the short time in which the diffusion of hydrogen can take place. In comparison with electron beam welding, even though this process offers the advantages of a high energy density welding process, a vacuum chamber is required, which is not always practical.

All advantages explain their integration in the advanced technology industries such as in aerospace, aircraft, automotive, electronics and other industries. Indeed, today, laser beam welding is being used in an increasingly wider range of industries, from the production of medical devices and microelectronics to shipbuilding. The automotive industry, in particular, takes advantage of this technology's benefits: low heat input, small heat-affected zone (HAZ), low distortion rate, good repeatability, reduced need for post processing and high welding speed. This last point is becoming critical for a successful application in the automotive industry because the increase in welding speed provided by laser welding has resulted in the need for an automated system. Another application of the laser process is the aircraft where weight and cost reduction in civil aircrafts by replacing rivets by advanced welding techniques has now been realized for skin-stringer joints. In this context the laser beam welding technology has proved to be very suitable for a number of reasons, for example, low distortion while processing at high speeds. These benefits have made laser welding the process of choice for many applications that previously used resistance welding. Compared for example with TIG welding, the welding speed with laser is generally three times higher.

However, although laser materials processing has gained widespread acceptability, the mechanisms and main factors controlling the process remain controversial and need further theoretical and experimental studies. Further work is needed to develop the weld process parameters necessary to achieve the materials characteristics required for the use of magnesium alloys in industrial applications. Improved gas shielding requirements are expected to be critical to obtaining welds with the required materials properties. Further studies are needed to determine the parameters controlling weld quality. Indeed, laser beam welding involves many variables: laser power, welding speed, defocusing distance and type of shielding gas, any of which may have an important effect on heat flow and fluid flow in the weld pool. This in turn will affect penetration depth, shape and final solidification structure of the fusion zone. These final states affect the mechanical behaviour. It is for that

this technique stays still in the developing stage and many mechanisms need to be studied because of many parameters which govern this process. However, with a good optimization, laser welding for the magnesium alloys seems to be the most appropriated joining technique and can promote their wider uses in aerospace, aircraft, automotive, electronics and other industries.

6. References

Agnew S.R., Duygulu Ö. (2005). Plastic anisotropy and the role of non-basal slip in magnesium alloy AZ31B. *International Journal of Plasticity*, Vol. 21, Issue 6, pp. 1161-1193.

Cao, X., Jahazi, M., Immarigeon, J.P., Wallace, W. (2006). A review of laser welding techniques for magnesium alloys. *Journal of Materials Processing Technology,* Vol. 171, pp. 188–204.

Cevat Sarioglu C. (2006). The effect of anisotropy on residual stress values and modification of Serruys approach to residual stress calculations for coatings such as TiN, ZrN and HfN. *Surface and coatings technology*, Vol. 201, Issue 3- 4, pp.707-717.

Cho, J.R., Conlon, K.T., Reed, R.C. (2003). Residual Stresses in an Electron Beam Weld of Ti-834: Characterization and Numerical Modelling. *Metallurgical and Materials Transactions A*, vol. 37, Issue 2, pp. 2935-2946.

Coelho, R.S., Kostka, A., Pinto, H., Riekehr, S., Koçak, M., Pyzalla, A.R. (2008). Microstructure and mechanical properties of magnesium alloy AZ31B laser beam welds. *Materials Science and Engineering A*, Vol. 485, Issue 1-2, pp.20–30.

D'Annessa, A. T. (1970). Sources and effects of growth rate fluctuation during weld metal solidification. *Welding Journal*, Vol. 49, Issue 2, pp 41–45.

Dai, K., Shaw L. (2003). Finite-Element Analysis of Effects of the Laser-Processed Bimaterial Component Size on Stresses and Distortion. *Metallurgical and Materials Transactions A*, vol. 37A, Issue 2, pp. 1133-1145.

Dhahri, M., Masse, J.E, Mathieu, JF, Barreau, G, Autric, M. (2000). CO_2 laser welding of magnesium alloys. *In Proceedings of the SPIE: High power lasers in manufacturing*, pp. 725–732.

Dhahri, M., Masse, J.E, Mathieu, JF, Barreau, G, Autric, M. (2000). CO_2 laser welding of magnesium alloys. *In Proceedings of the SPIE: High power lasers in manufacturing*, pp. 725–732.

Dhahri, M., Masse, J.E, Mathieu, JF, Barreau, G, Autric, M. (2001). Laser weldability of WE43 magnesium alloys for aeronautic industry. *In third LANE 2001: Laser Assisted Net Shape Engineering*, pp. 297–310,

Dhahri, M., Masse, J.E, Mathieu, JF, Barreau, G, Autric, M. (2001). Laser welding of AZ91 and WE43 magnesium alloys for automotive and aerospace industries. *Advanced engineering materials*, Vol. 3, Issue 7, pp. 504–507, 2001.

Dhahri, M., Masse, J.E, Mathieu, JF, Barreau, G, Autric, M. (2002). Laser welding of magnesium alloys for automotive and aerospace applications. *http://webdb.dgm.de/dgm lit/*, October 2002.

Dong, W., Kokawa, H., Tsukamoto, S., Sato Y. S., Ogawa, M. (2004). Mechanism governing nitrogen absorption by steel weld metal during laser welding. *Metallurgical and Materials Transactions B*, pp. 331-338.

Dubé, D., Fiset, M., Couture, A., Nakatsugawa, I. (2001). Characterization and performance of laser melted AZ91D and AM60B. *Materials science and Engineering A*, vol. 299, pp. 38-45.

Haferkamp, H., Bach, Fr.-W., Burmester, I., Kreutzburg, K., Niemeyer, M. (1996). Nd:YAG laser beam welding of magnesium constructions. *In Proceedings of the Third International Magnesium Conference, UMIST,* Manchester, UK, 10–12 April 1996, pp. 89–98.

Haferkamp, H., Dilthey, U., Trager, G., Burmester, I., Niemeyer, M. (1998). Beam welding of magnesium alloys. *In Proceedings Conference: Magnesium Alloys and Their Applications*, Wolfsburg, Germany, 28–30 April 1998, pp. 595–600.

Hiraga, H., Inoue, T., Kamado, S. Kojima, Y. (2001). Effect of the shielding gas and laser wavelenght in laser welding magnesium alloy sheet. *Quart. J. Weld. Soc*., Vol. 19, Issue 4, pp. 591–599.

Hsiao, I.C., Su, S.W., Huang, J.C. (2000). Evolution of texture and grain misorientation in an Al-Mg alloy exhibiting low-temperature superplasticity. *Metallurgical and Materials Transactions A*, Vol. 33, Issue 5, pp. 2169-2180.

Jensen, M.V.R. S., Dye, D., James, K. E., Korsunsky, A. M., Roberts, S. M., Reed R. C. (2002). Residual stresses in a welded superalloy disc : characterization using synchrotron diffraction and numerical process modelling. *Metallurgical and Materials Transactions A*, Vol. 37, Issue 2, pp. 2921-2931.

Kalinyuk, A.N., Trigub, N.P, Zamkov, V.N., Ivasishin, O.M., Markovsky, P.E, Teliovich, R.V., Semiatin, S.L. (2003). Microstructure, texture, and mechanical properties of electron-beam melted Ti-6Al-4V. *Materials Science and Engineering A*, Vol. 346, pp. 178-188.

Kouadri A., Barrallier L. (2011). Study of mechanical properties of AZ91 magnesium alloy welded by laser process taking into account the anisotropy: micro-hardness and residual stresses by X-ray diffraction., *Metallurgical and Materials Transactions A*, Vol. 42, Issue 7, pp. 1815-1826.

Kouadri, A., Barrallier, L. (2006). Texture characterization of hexagonal metals: magnesium AZ91 alloy, welded by laser processing. *Materials science and Engineering A*, Vol. 429, Issues 1-2, pp. 11- 17.

Kurtz, W., Bezençon, C., Gäumann, M. (2001). Columnar to equiaxed transition in solidification processing. *Science and Technology of Advanced Materials*, Vol. 2, pp. 185-191.

Lehner, C., Reinhart, G., Schaller, L. (1999). Welding of die cast magnesium alloys for production. *J. Laser Appl*. Vol. 11, Issue 5, pp. 206–210.

Leong, K.H., Sanders, P.G., Keske, J.S., Kornecki, G. (1998). Laser beam welding of AZ31BH24 alloy. *ICALEO 98: Laser Material processing conference*, Orlando, FL, 16-19 November 1998, pp. 28–36.

Liu, S., Edwards, G.R., Olson, D., Marya, M. (2000). Laser processing research at the Colorado School of Mines. *In Asian Pacific Welding Conference: Proceedings NZIW 2000 Annual Conference and WTIA 48th Annual Conference*, Melbourne, 29 October to 2 November 2000, pp. 1–18.

Luo, A. (1996). Heterogeneous nucleation and grain refinement in cast Mg(AZ91)/SiCp metal matrix composites. *Canadian Metallurgical Quarterly*, Vol. 35, pp. 375-383.

Mao, W.G., Zhou, Y.C., Yang L., Yu, X.H. (2006). Modeling of residual stresses variation with thermal cycling in thermal barrier coatings. *Mechanics of materials*, Vol.38, Issue 12, pp. 1118-1127.

Marya, M., Edwards, G.R. (2001). Factors controlling the magnesium weld morphology in deep penetration welding by a CO_2 laser. *Journal of Materials Engineering and Performance*, Vol. 10, Issue 4, pp.435–443,

Marya, M., Edwards, G.R. (2000). The laser welding of magnesium alloy AZ91. *Weld. world*, Vol. 44, Issue 2, pp.31–37.

Matysina, Z.A. (1999). The relative surface energy of hexagonal close-packed crystals. *Materials Chemistry and Physics*, Vol. 60, pp. 70-78.

Pastor, M., Zhao, H., DebRoy, T. (2000). Continuous wave- Nd:yttrium–aluminium–garnet laser welding of AM60B magnesium alloys, *J. Laser Appl.*, Vol. 12, Issue 3, pp. 91–100.

Pina, J. Dias, A., François, M., Lebrun, J.L. (1997). Residual stresses and crystallographic texture in hard-chronium electroplated coatings. *Surface and coatings technology*, Vol. 96, pp.148-162.

Pryds N.H., Huang, X. (2000). The effect of cooling rate on the microstructures formed during solidification of ferritic steel. *Metallurgical and Materials Transactions A*, Vol. 33, Issue 5, pp. 3155-3166.

Sanders, P.G., Keske, J.S., Leong, K.H., Kornecki, G. (1999). High power Nd:YAG and CO2 laser welding of magnesium. *J. Laser Appl.*, Vol. 11, Issue 2, pp. 96–103.

Shaw, C., Jones, H. (1997). The contributions of different alloying additions to hardening in rapidly solidified magnesium alloys. *Materials Sciences and Engineering A,* Vol. 226-228, pp. 856-860.

StJohn, D.H., Dahle, A.K., Abbott, T., Nave M.D., Qian, M. (2003).Solidification of cast magnesium alloys. *The minerals, Metals and Materials Society*, pp. 95-100.

Su, S.F., Huang, J.C., Lin, H.K., Ho N.J. (2002). Electron-Beam Welding Behavior in Mg-Al-Based Alloys. *Metallurgical and Materials Transactions A*, Vol. 33, Issue 5, pp. 1461-1473.

Teng, T.L, Fung C.H., Chang, P.H. (2002). Effect of weld geometry and residual stresses on fatigue in butt-welded joints. *International Journal of Pressure Vessels and Piping*, Vol. 79, Issue 7, pp. 467-482.

Wagner, L. (1999). Mechanical surface treatments on titanium, aluminum and magnesium alloys. *Materials Science and Engineering A,* Vol. 263, Issue 2, pp. 210-216.

Wang H.Y., Li, Z.J. (2006). Investigation of laser beam welding process of AZ61 magnesium based alloy. *Acta metallurgica sinica (english letters)*, Vol. 19, Issue 4, pp. 287–294.

Watkins, K.G. (2003). Laser welding of magnesium alloys. *In H.I. Kaplan, editor, Magnesium Technology, TMS Annual Meeting and Exhibition*, pp. 153–156, San Diego.

Weisheit, A., Galun, R., Mordike, B.L. (1997). Weldability of various magnesium alloys using a CO2 laser, *IIW seminar, Trends Weld, Lightweight automobile railroad vehicles*, pp. 28–41.

Weisheit, Galun, R., Mordike, B.L. (1998). CO2 laser beam welding of magnesium-based alloys. *Weld. Res. Suppl.*, Vol. 74, Issue 4, pp. 149–154.

Wu, X., Kalidindi, S. R., Necker, C., Salem, A.A. (2007). Prediction of crystallographic texture evolution and anisotropic stress–strain curves during large plastic strains in

high purity titanium using a Taylor-type crystal plasticity. *Acta Materialia*, Vol.55, pp. 423-432.

Zhao, H., DebRoy, T. (2001). Pore formation during laser beam welding of die cast magnesium alloy AM60B – mechanism and remedy. *Weld. J.*, Vol. 80, Issue 8, pp. 204S–210S.

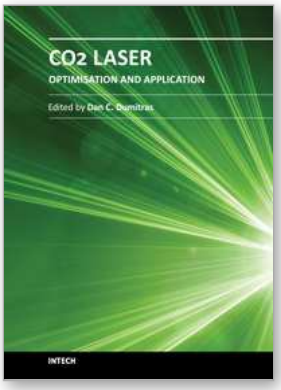

CO2 Laser - Optimisation and Application

Edited by Dr. Dan C. Dumitras

ISBN 978-953-51-0351-6
Hard cover, 436 pages
Publisher InTech
Published online 21, March, 2012
Published in print edition March, 2012

The present book includes several contributions aiming a deeper understanding of the basic processes in the operation of CO2 lasers (lasing on non-traditional bands, frequency stabilization, photoacoustic spectroscopy) and achievement of new systems (CO2 lasers generating ultrashort pulses or high average power, lasers based on diffusion cooled V-fold geometry, transmission of IR radiation through hollow core microstructured fibers). The second part of the book is dedicated to applications in material processing (heat treatment, welding, synthesis of new materials, micro fluidics) and in medicine (clinical applications, dentistry, non-ablative therapy, acceleration of protons for cancer treatment).

InTech Europe
University Campus STeP Ri
Slavka Krautzeka 83/A
51000 Rijeka, Croatia
Phone: +385 (51) 770 447
Fax: +385 (51) 686 166
www.intechopen.com

InTech China
Unit 405, Office Block, Hotel Equatorial Shanghai
No.65, Yan An Road (West), Shanghai, 200040, China
中国上海市延安西路65号上海国际贵都大饭店办公楼405单元
Phone: +86-21-62489820
Fax: +86-21-62489821